Structural Chemistry (2024) 35:841–852
https://doi.org/10.1007/s11224-023-02239-4

RESEARCH

Molecular docking, expounding the regiospecificity, stereoselectivity, and the mechanism of [5+2] cycloaddition reaction between ethereal ether and oxidopyrylium

Anas Ouled Aitouna[1,2] · Noureddine Mazoir[2] · Abdellah Zeroual[1] · Asad Syed[3] · Ali H. Bahkali[3] · Abdallah M. Elgorban[3] · Meenakshi Verma[4] · Mohammed El idrissi[5] · Radomir Jasiński[6]

Received: 5 August 2023 / Accepted: 3 October 2023 / Published online: 12 October 2023

Abstract
Application of molecular electron density theory (MEDT) to investigate the [5+2] cycloaddition reaction between oxidopyrylium and ethervinylether, we discovered that oxidopyrylium is an electrophile and ethervinylether is a nucleophile by an examination of conceptual DFT indices. Analysis of energetical parameters shows clearly that this cycloaddition is both regio- and stereoselective, which is extremely consistent with the experience. Topological analysis of the electron localization function (ELF) has shown that this [5+2] cycloaddition is achieved by a two-step, single-step mechanism along the most favored route. Aside from that, docking outcomes show that the (**1**–**20**) oxabicyclo[3.2.1]octene derivatives have a significant anti-HIV potential.

Keywords [5+2] cycloaddition · MEDT · Regiospecificity · DFT · ELF · Oxidopyrylium

Introduction

Cycloaddition reactions represent a valuable synthetic tool for the formation of carbo- and heterocyclic structures, often with high regio- and stereo-control [1]. Cycloaddition reactions, such as [4+2] Diels-Alder cycloaddition [2–5], [2+1] cycloaddition [6–9], and [3+2] cycloaddition [10–16], considered powerful tools for the construction of six-, three-, and five-membered rings, respectively, are heavily studied, and the literature contains numerous theoretical and experimental studies on these types of reactions [17–25]. On the contrary, there is comparatively much less work on the formation of seven-membered rings. Seven-membered rings are structural units widely present in a wide range of natural biologically active compounds. These chemicals can be found, for example, in rubriflordilactone A [26], phomarol [27], and cortistatin A [28]. Given the increase in natural compounds containing seven-membered rings which have been isolated with biological activity, it has become necessary to find and develop synthesis of these molecules utilizing successful synthetic methods, among these strategies are metathesis, cyclizations, ring isomerization, and cycloadditions [29], but synthesis of these rings is difficult and challenging, due to unfavorable entropy in cyclization processes [30]. Cycloaddition reactions represent an efficient and direct protocol for accessing seven-membered rings, primarily the [5+2] cycloaddition (52CA) reaction [31, 32] and the [4+3] cycloaddition reaction [33, 34]. However, due to the variety of forms, the final scenario is preferred to the cycloaddition [4+3] for the creation of rings with seven

✉ Mohammed El idrissi
m.elidrissi2018@gmail.com

1 Molecular Modelling and Spectroscopy Research Team, Faculty of Science, Chouaïb Doukkali University, P.O. Box 20, 24000 El Jadida, Morocco

2 Laboratory of Bioorganic Chemistry, Department of Chemistry Faculty of Sciences, Chouaïb Doukkali University, P. O. Box 20, 24000 El Jadida, Morocco

3 Department of Botany and Microbiology, College of Science, King Saud University, P.O. Box 2455, 11451 Riyadh, Saudi Arabia

4 University Centre for Research & Development, Department of Chemistry, Chandigarh University Gharuan, Mohali, India

5 Team of Chemical Processes and Applied Materials, Faculty Polydisciplinary, Sultan Moulay Slimane University, Beni-Mellal, Morocco

6 Department of Organic Chemistry and Technology, Cracow University of Technology, Warszawska 24, 31-155 Cracow, Poland

Scheme 1 The oxidopyrylium cycloaddition reaction

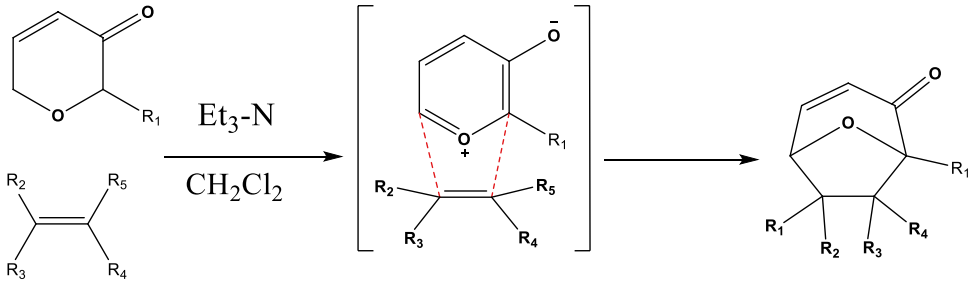

chains 52CA. There are several types of 52CAs reactions based on the five-membered component involved in the reaction [35]. The 52CA reactions between an oxidopyrylium and alkenes allow for the simultaneous generation of bridged bicyclic ethers and the seven-membered ring compounds, which are a structural basis present in biologically active natural products [36]. Most commonly, the oxidopyrylium cycloaddition reaction begins with the formation of an oxidopyrylium zwitterionic intermediate through the removal of the acetoxy group from the acetoxypyrone precursor to the oxidopyrylium in the presence of alkenes [37] (Scheme 1). The formation of oxidopyrylium could also be obtained from acetoxypyrone using a base [38].

There has not been much theoretical study of the [5+2] cycloaddition reaction of oxidopyrylium with alkenes [39–41], compared to the [4+2] and [3+2] cycloaddition reactions, which are widely studied by various theoretical models of chemical reactivity [42–45].

One of the most widely used and robust reactivity models in recent years is Domingo's so-called MEDT theory. In 2016, Domingo introduced the molecular electron density theory (MEDT), a novel theoretical framework for describing reactivity in organic chemistry [46], regarding organic molecules' reactivity is related to changes in electron density, in complete disagreement with all models based on molecular orbital analysis, such as boundary molecular orbital theory [47, 48]. In addition to investigating and characterizing the energetically relevant reaction pathways associated with the process under study, the reactivity indices produced from the CDFT, topological analysis methods ELF (electron localization function) [49], QTAIM [50], and NCI [51], are employed in the current study to examine the reactivity inside the MEDT, we are particularly interested in the [5+2] cycloaddition of oxidopyrylium with an alkene (Scheme 2 and Fig. 1).

Computation methods

The optimization of the geometry of reactants, products, and transition states was performed by DFT computations applying the ωB97XD functional; it is an extension of the widely used B97-D functional and includes empirical dispersion corrections, which are designed to better account for van der Waals interactions in molecular systems, coincidentally with 6-311G(d,p) basis [52]. Frequency calculations were used to characterize optimized stationary positions to make sure that none of the reactants or products had any imaginary frequencies, and that the transition states have just one imaginary frequency. Intrinsic reaction coordinate (IRC) [53] paths were plotted in both directions, with the aim of verifying the energy profiles linking each transition stage to its two corresponding minimum. By employing the Tomasi group polarizable continuum model (PCM) to re-optimize the stationary points obtained in the gas phase, the solvent impact of dichloromethane was implicitly taken into account [54].

The global electrophilicity index was calculated using the equation shown below [55]:

$$\omega = \frac{\mu^2}{2\eta}$$

wherein the electronic chemical potential and chemical hardness are represented by μ and η, respectively, the two quantities μ and η according to the aforementioned formulas, they were calculated utilizing the HOMO and LUMO values [55–58]:

$$\mu = \frac{E_{HOMO} + E_{LUMO}}{2}$$

and

Scheme 2 [5+2] cycloaddition of oxidopyrylium with an alkene

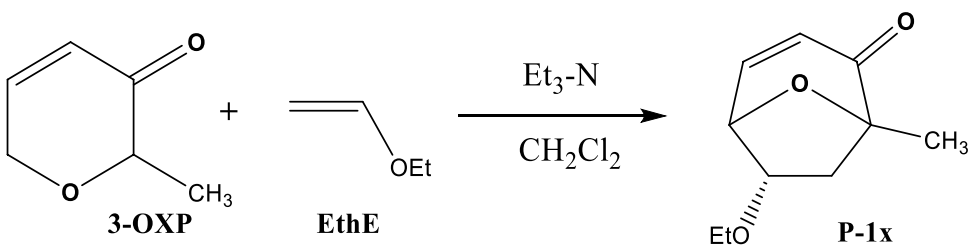

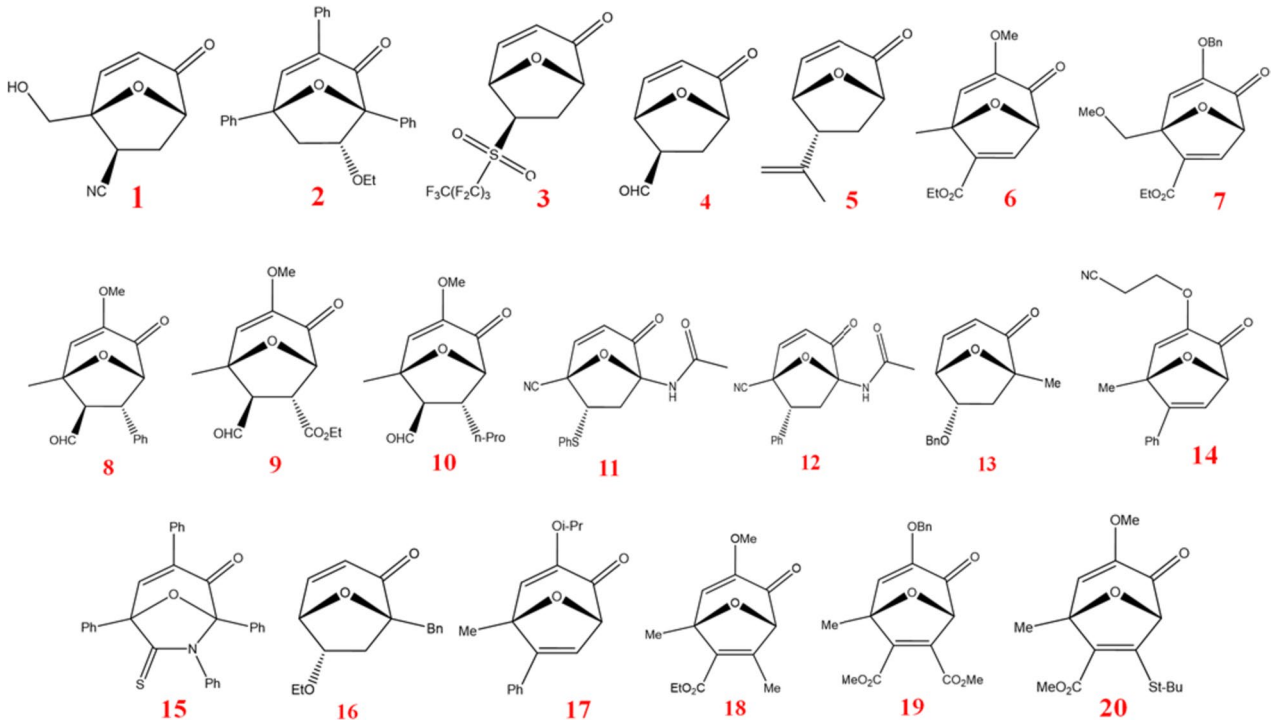

Fig. 1 [5+2] cycloaddition of oxidopyrylium with an alkene

$$\eta = E_{LUMO} - E_{HOMO}$$

The overall nucleophilicity index N was calculated according to the following formula:

$$N = E_{HO}(Nu) - E_{HO}(TCE)$$

with $E_{HO}(Nu)$ corresponds to the HOMO energy of the reagent and tetracyanoethylene's HOMO energy is known as $E_{HO}(TCE)$ [58].

All reactivity indices were evaluated utilizing B3LYP/6-31G(d) level in accordance with Domingo's suggestions [59, 60].

The total of the naturally found atomic charges (q), as determined by a natural population analysis (NPA), was used to calculate the overall GEDT [61] electron density transfer of the atoms belonging to each reactant (f) at the transition state $GEDT = \sum q_f$. The Topmod program has been employed to undertake a topological inquiry of the ELF electronic localization function [62]. The GaussView software was utilized for visualizing the locations of the ELF pool attractors [63], while the VMD program was applied to illustrate the ELF pool isosurfaces [64] with an isovalue of 0.82.

Result and even discussion

Comparison of the **3-OXP 2** and **EthE** ground-state electronic structures' global and local reactivity indices obtained via CFDT.

Table 1 lists the computed global reactivity indices for **3-OXP** and **EthE**, including electronic chemical potential (μ), chemical hardness (η), electrophilicity (ω), and nucleophilicity (N). The geometry of **3-OXP** and **EthE** has been entirely optimized at this level since these indices have been scaled to the computational level of B3LYP/6-31G(d), with the goal of having complete consistency with the scale suggested by Domingo [59, 60].

According to an analysis of the data in Table 1, **EthE** (−2.39 eV) has a lower electronic chemical potential (ECP) than **3-OXP** (−3.75 eV), which indicates that during a polar reaction, the electron density will transfer from **EthE**, which acts as a nucleophile, to **3-OXP**, which acts as an electrophile. Domingo divided nucleophiles into three categories: strong, moderate, and marginal, with respective nucleophilicity indices of 3.00, 2.00–3.00, and less than 2.00 eV. Similar to this, electrophiles are likewise divided into three groups: strong, moderate, and marginal, depending on their electrophilicity indices, which range from 1.50 to 0.80 eV,

Table 1 Derived for **3-OXP** and **EthE** are the global electronic qualities (global electrophilicity (ω), global nucleophilicity (N), global electrochemical potential (μ), and chemical hardness (η)) calculated by B3LYP/6–31(d)

System	μ	η	ω	N
3-OXP	−3.75	3.36	2.09	4.09
EthE	−2.39	6.98	0.41	3.64

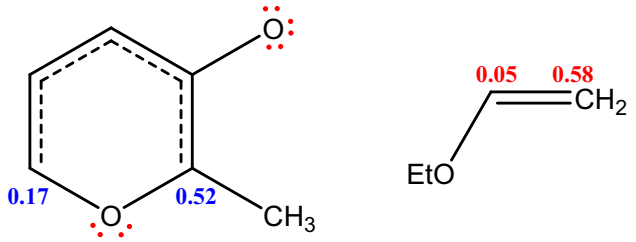

Fig. 2 The electrophilic Parr function P_k^+ of **3-OXP** and the nucleophilic Parr function P_k^- of **EthE**

1.50 to 0.80 eV, and 0.80 eV and lower, respectively. This scale classifies **3-OXP** as both a strong electrophile with a value of 2.09 eV and a strong nucleophile with a value of 4.09 eV. **EthE** is categorized as both a very poor electrophile with a value of 0.41 eV and a strong nucleophile with a value of 3.64 eV.

Regarding local reactivity, Domingo et al. suggested two new functions called electrophilic and nucleophilic Parr's functions, to pinpoint among the most nucleophilic and electrophilic centers in the species. According to the examination of the nucleophilic Parr functions of **EthE**, the carbon C1, $P_{C1}^- = 0.58$, is the most nucleophilic center, whereas the **3-OXP**'s electrophilic Parr functions reveal that the C4 carbon is this molecule's highest electrophilic center, with a $P_{C4}^+ = 0.52$ value, and is three times larger than the C6 carbon, with a $P_{C6}^+ = 0.17$ value (Fig. 2).

The analysis of Parr functions leads to the conclusion that the C1 carbon of **EthE** and the C4 carbon of **3-OXP** will have the best electrophile–nucleophile interaction along the nucleophilic attack of **EthE** on **3-OXP**, suggesting that this reaction will primarily proceed via the C1-C4 regioisomeric pathway in clear agreement with experimental observations.

ELF enquiry of reagents 3-OXP and EthE

Positions of the valence attractors with their populations, localization domain, and suggested Lewis structures for the two reactants **3-OXP** and **EthE** are shown in Fig. 3.

Figure 3 shows that the oxygen atom of **3-OXP** has two monosynaptic pools, V(O1) and V′(O1), with a combined population of 5.59 electrons. Additionally, the oxygen atom of O5 has a monosynaptic pool, V(O5), with a population of 3.67 electrons, which is indicative of two free electron doublets carried by the oxygen O5.

The presence of two disynaptic pools with electron populations of 1.88e and 1.78e, V(O5,C4) and V(O5,C6), respectively, values close to 2e, signifying an O5-C4, O5-C6 single bond, as well as a disynaptic pool V(O,C3) with a population of 2.04e, indicates an O-C3 single bond. In addition, the presence of four disynaptic pools, with electron populations of 2.54, 2.96, 2.96, and 3.27e values greater than 2e and less than 4e, suggests a single bond with a double bond character; on the other hand, the ELF analysis of **EthE** reveals the presence of two disynaptic pools, V(C1,C2) and V′(C1,C2), with a combined population of 3.71e, suggesting a remarkable character of a double bond. Additionally, we observe that the oxygen atom of **EthE** has two monosynaptic pools, V(O)

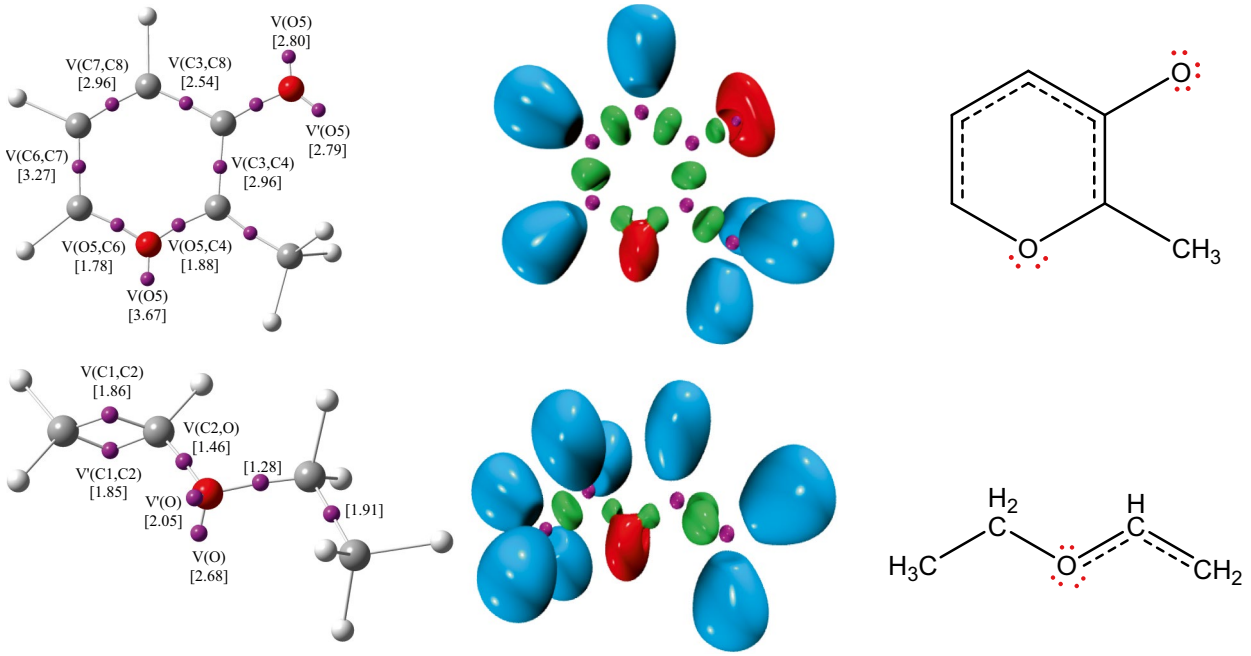

Fig. 3 Positions of the **3-OXP** and **EthE** reactants' valence attractors, as well as their respective populations, localization domains, and Lewis structures

and V′(O), with a combined population of 4.73e, which may be bound to two pairs of this atom's non-bonding electrons.

The disynaptic pool V(C2,O), which has a population of 1.46e but is unexpected compared to the expected value of 2e, is present in the C2-O binding region. This depopulation of the C2-O binding region in the direction of the oxygen atom can also be attributed to the disynaptic pool, which has a population of 1.28e.

Energetics study of the 52CA reaction between 3-OXP and EthE

Due to the non-symmetry of the two reactants, there are four possible isomeric paths for the 52CA reaction of **3-OXP** with **EthE**: two regioisomeric pathways, each of which produces two stereoisomers.

The C1-C4 single bond creation pathway and the C1-C6 single bond initiation pathway are a pair of regioisomeric pathways, whereas stereoisomeric pathways named exo and endo depending on the position between the methyl group affixed to the C4 carbon of **3-OXP** and the ethoxy group of **EthE**, such that along the exo pathway, the two ethoxy and methyl groups are on opposite sides. This 52CA reaction exhibits a one-step mechanism, i.e., on the reaction's surface potential energy, a single TS, **TS-1x**, **TS-1n**, **TS-2x**, and **TS-2n**, as well as their associated cycloadducts, **P-1x**, **P-1n**, **P-2x**, and **P-2n**, have been identified and characterized (Scheme 3).

Table 2 ωB97XD/6-311G(d,p) relative electronic energies (in kcal·mol^{-1}), in the gas phase and in the presence of dichloromethane, for the species involved in the 52CA reaction between **3-OXP** and **EthE**

	Gas phase	Solution (DCM)
TS-1x	2.1	3.3
TS-1n	5.0	6.7
TS-2x	3.9	6.8
TS-2n	6.6	9.0
P-1x	−48.5	−44.4
P-1n	−48.4	−44.8
P-2x	−47.6	−44.3
P-2n	−47.5	−43.5

Table 2 lists the relative electron energies for the species involved in the reaction of 52CA between **3-OXP** and **EthE**, both in the gas phase plus when dichloromethane is present, while the detailed calculation in gas and DCM are presented in Tables S1 and S2.

The four competitive routes have gas phase activation energies of 2.1 (**TS-1x**), 5.0 (**TS-1n**), 3.9 (**TS-2x**), and 6.6 (**TS-2n**) kcal/mol. The results presented here indicate that the 52CA reaction is highly stereoselective and slightly regioselective because **TS-1x** has a lower energy than **TS-2x** of 1.8 kcal/mol and **TS-1x** has a lower energy than **TS-1n** of 2.9 kcal/mol. This reaction can also be regarded as irreversible because of the strong exothermic between 47.6 and 48.5 kcal/mol.

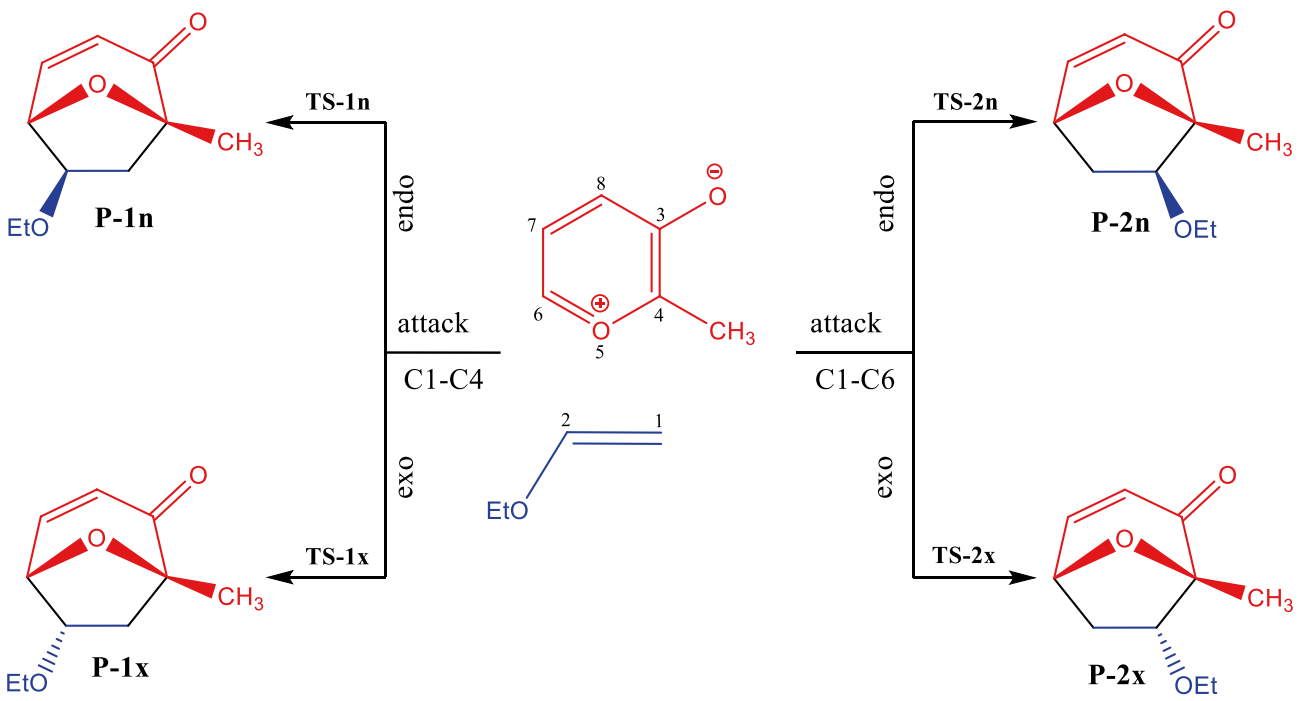

Scheme 3 Theoretical potential regio- and stereoisomeric reaction paths for the 52CA reaction involving **3-OXP** and **EthE**

Counting dichloromethane as a solvent, the activation energies increase to 3.3 (**TS-1x**), 6.7 (**TS-1n**), 6.8 (**TS-2x**), and 9.0 (**TS-2n**) kcal/mol, due to a strong solvation of reactants with respect to transition states. The gas phase's regioselectivity does not alter, but has improved, since the most favorable **TS-1x** has an energy 3.5 kcal/mol inferior than **TS-2x**, as well as the stereoselectivity increases, since **TS-1x** is more stable 3.4 kcal/mol than **TS-1n**.

Figure 4 illustrates the geometries of the transition states involved in the 52CA reaction between **3-OXP** and **EthE**.

The four transition states correspond to asynchronous single bond formation processes, according to an examination of the geometries of the transition states involved in the reaction of 52CA between **3-OXP** and **EthE**. More progress has been made in the formation of the single bond involving the C1 carbon of **ETHE** than the C2 carbon. Compared to C2-C6, the formation of the C1-C4 bond is further along. Dichloromethane's two formed bonds' different lengths provide as evidence that these transition stages have grown increasingly asynchronous. The most asynchronous transition stage, **TS-1x**, is also the most advantageous.

By computing the GEDT values of the four transition states, it was then possible to determine whether the 52CA reaction under investigation was polar or nonpolar. Nonpolar processes are reactions with GEDT values less than 0.0e, while polar processes are reactions with GEDT values higher than 0.2e. The values of GEDT from **EthE** to **3-OXP** are 0.18e at **TS-1x**, 0.12e at **TS-1n**, 0.08 at **TS-2n**, and 0.10 at **TS-2x**, demonstrating the weak polarity of this 52CA reaction.

ELF analysis to ascertain the 52CA reaction's chemical mechanism

Through performing an ELF topological analysis on a few chosen spots of the IRC of the most advantageous transition state, **TS-1n**, it was possible to obtain insight into the chemical mechanism of the 52CA reaction involving **3-OXP** and **EthE**.

This ELF analysis will allow us to detect successive changes in the selected points' electron densities. The IRC profile of **TS-1n** consisted of a total of 250 points in the forward and reverse directions. The positions of ELF valence attractors along with their corresponding populations of relevant structures are shown in Fig. 5.

Despite the modest variations in their electron populations, the ELF valence patterns of the interacting fragments at the initial point P1—where they are significantly separated from one another—resemble those of the two separate reactants **3-OXP** and **EthE**. The depopulation of the disynaptic basin V′(C1,C2) begins at position **P2**. A new monosynaptic basin V(C4) with an initial electron population of 0.31e has developed at point **P3**. Point **P4** sees the formation of a novel monosynaptic pool, V(C1), with an initial

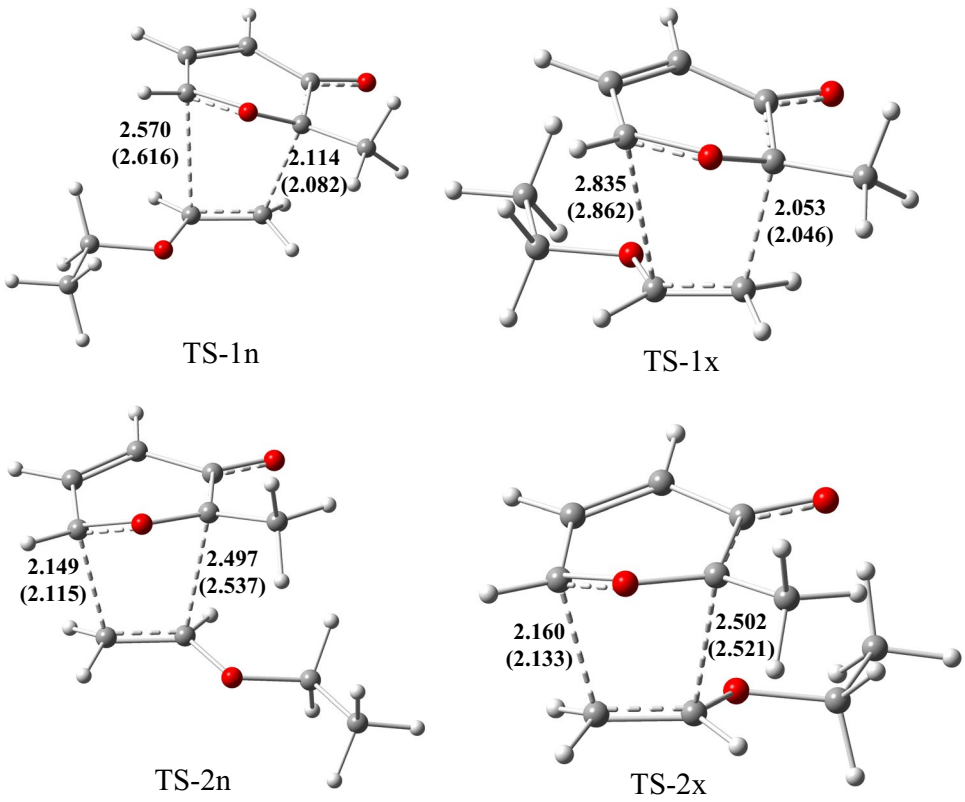

Fig. 4 The optimized transition state geometries connected to the 52CA reaction between **3-OXP** and **EthE**. The units of measurement are angstroms. In brackets, the dichloromethane values are listed

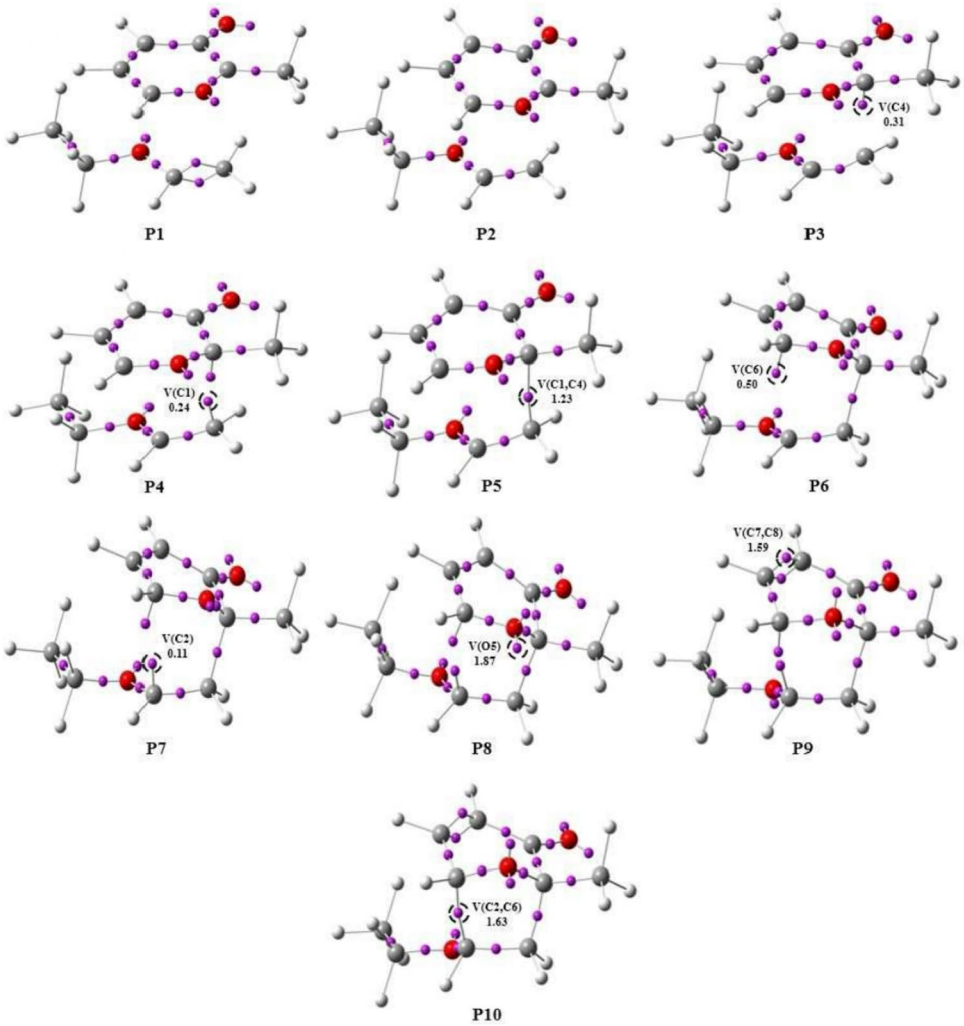

Fig. 5 Positions of ELF valence attractors with their populations of relevant structures

population of 0.24e. It is confirmed that the C1-C4 bond forms before the C2-C6 bond at point **P5** due to the disappearance of the two monosynaptic basins V(C1) and V(C4) and the emergence of a new disynaptic basin V(C1,C4) with an initial population of 1.23e. A new monosynaptic pool V(C6) on carbon C6 with an initial electronic population of 0.50e is formed at point **P6**, while a monosynaptic pool V(C2) on carbon C2 with an initial electronic population of 0.11e is formed at point **P7**. Due to the depopulation of V(O5) at point **P8**, a new monosynaptic pool V′(O5) with an initial population of 1.87e is formed on the oxygen atom O5. A second disynaptic pool, V′(C7,C8), formed at point **P9** with an initial electronic population of 1.59e, demonstrating the production of the C7 = C8 double bond. The two monosynaptic pools V(C2) and V(C6) fuse at point **P10**, resulting in the formation of the C2-C6 single bond and a disynaptic pool V(C2,C6) with an initial population of 1.63e. According to these findings, the 52CA reaction between **3-OXP** and **EthE** proceeds via a one-step, two-phase mechanism, in which the two new single bonds are formed between the two reactants in an uncoordinated environment and the formation of the C1-C4 bond is advanced in comparison to the formation of the C2-C6 bond.

Molecular docking

As a powerful tool for assisting the development of potential medications for a wide range of ailments, computer-aided drug design (CADD) based on ligand and structure-based processes such as 3D-QSAR, pharmacophore, molecular docking, and ADMET has evolved [65]. The retrovirus family, which includes the human immunodeficiency virus (HIV), which causes acquired immunodeficiency syndrome (AIDS), assaults immune system cells by destroying or weakening their functioning [66]. It is still crucial to find new medications with antiviral properties, as HIV mutates rapidly, leading to treatment ineffectiveness and the development of drug-resistant strains. Protein Data Bank (http://www.rcsb.org) was used to retrieve the target HIV-1 protease protein's three-dimensional (3D) crystal structure prior to

docking. To examine substituted (**1**–**20**) oxabicyclo[3.2.1] octene derivatives' interactions with the HIV-1 protease (PDB ID: 1HSG) protein, a molecular docking simulation was conducted using the AutoDock 4.2.6 program and the graphical interface AutoDockTools (ADT) version 1.5.6 [67]. Prior to the docking process, the 1HSG protein's water molecules and polar hydrogen atoms were removed. Next, Kollman and Gasteiger atom charges were added using ADT. The central grid box is approximately (13.073, 22.467, and 5.557) based on the ligand position in the protein, and the grid maps were constructed to 60 in the X, Y, and Z dimensions. Software programs called PyMOL and Discovery Studio Visualizer were employed to demonstrate the potential binding processes of the oxabicyclo[3.2.1]octene derivatives with their target proteins and visually check the docked molecule and its H-bond interactions in an effort to explain their anti-HIV-1 effects, respectively [68, 69].

Figures S1 and S2 depict the results obtained on docking all the (**1**–**20**) oxabicyclo[3.2.1]octene derivatives with target 1HSG protein based on docking studies, while Fig. 6 depicts docking result of compound **5**. All the ligands interacted with key active site residues of the HIV-1 protease such as ASP29, ASP30, ILE50, GLY48, and ARG8. The docked molecules contain conventional hydrogen bonds that are mainly formed with oxygen atoms of oxabicyclo[3.2.1] octene and N atoms of C≡N group. The docking variables, which include intermolecular energy, inhibition constant, and binding energy of the (**1**–**20**) oxabicyclo[3.2.1]octene derivatives with the 1HSG targeted protein, were depicted in Table S3. The binding energies for all the substituted (**1**–**20**) oxabicyclo[3.2.1]octene derivatives with the HIV-1 protease (PDB ID: 1HSG) protein exhibited dock values between − 5.01 and − 8.73 kcal/mol. The order of binding energies in relation to the drug activeness against 1HSG is **15** > **2** > **11** > **17** > **14** > **19** > **12** > **7** > **20** > **13** > **8** > **16** > **6** = **18** > **10** > **5** > **9** > **3** > **1** > **4**. Compound **15** formed a strong conventional hydrogen bond with ARG8 (2.1 Å) and one van der Waals with ASP29 (4.1 Å) of 1HSG protein. The obtained results indicate that the (**1**–**20**) oxabicyclo[3.2.1] octene derivatives have high potential to act as anti-HIV agents. The docking findings could influence the design and development of novel AIDS medication candidates.

Computational pharmacokinetic analysis (physicochemical and ADME properties) of the (1–20) oxabicyclo[3.2.1]octene derivatives

The two main reasons why many drug candidates still fail to become drugs are the lack of efficacy and safety, which means that at every step of drug discovery and development, the properties of chemicals that affect absorption, distribution, metabolism, excretion, and toxicity (ADMET) are essential. The ADME analysis measures absorption, distribution, metabolism, and excretion; an online software tool was employed to examine the physicochemical, lipophilicity, water solubility, and pharmacokinetics, drug-likeness plus medicinal chemistry properties of the (**1**–**20**) oxabicyclo[3.2.1]octene derivatives. Using an online program called SwissADME, which is accessible at http://www.swissadme.ch, the ADME forecasts were made [70].

The "Rule of Five (Ro5)" or Lipinski's rule of five (5), developed by Christopher A. Lipinski in 1997 [71], is the

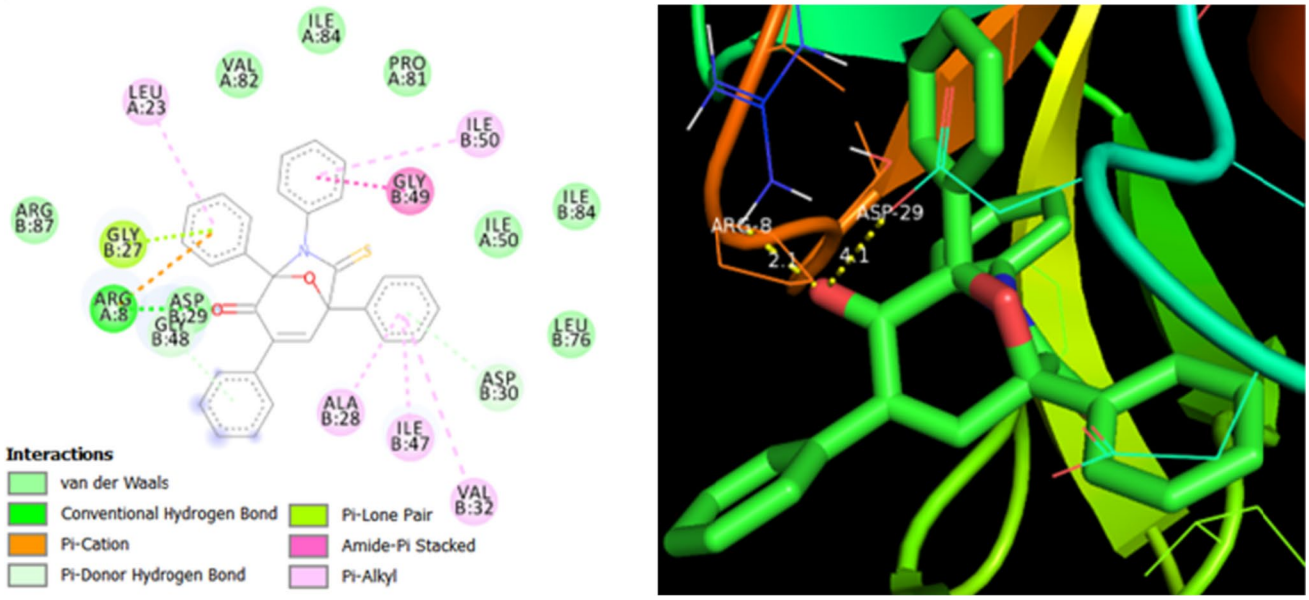

Fig. 6 2D and 3D diagrams of the (**15**) oxabicyclo[3.2.1]octene compounds docked in the anti-HIV-1 protein's binding site

first and best-known rule-based methodology to use when identifying chemicals as prospective therapeutic candidates. According to Lipinski's rule, active molecules should have a molecular weight (MW) of less than 500 g/mol, an octanol/water partition coefficient (iLOGP) of less than 5, a number of hydrogen bond acceptors (NHBA) of more than 10, a number of hydrogen bond donors (NHBD) of less than 5, and a topological polar surface area (TPSA) of more than 130 g/mol.

According to the rule of five, a compound cannot be orally active when two or more of Lipinski's rules of five are violated. All the (**1**–**20**) oxabicyclo[3.2.1]octene derivatives have no transgressions of the bioavailability score and Lipinski's rule of all the ligands showed a score of 55% (Table S4).

The bioavailability radar is employed to provide a preliminary assessment of a molecule's drug-likeness. The pink area must completely enclose the red line of the tested substance, indicating their drug-likelihood with a better bioavailability profile. The (**1**–**20**) oxabicyclo[3.2.1]octene derivatives are predicted orally bioavailable in Fig. S3. Six physicochemical indices, including lipophilicity (XLOGP3), size, polarity, solubility, flexibility, and saturation, were shown on the axis by the bioavailability radars. The two-dimensional bioavailability radar graphs of **15** compound show that the disadvantageous physicochemical property the deviation outside the pink area can be used to determine factors like saturation.

Solubility is an important property in the search for oral administration medications. The amount of water that may be dissolved is indicated in log (mol/l) (insoluble = 10, poorly soluble = 6, moderately soluble = 4, very soluble = 2, highly soluble = 0). The outcomes of the logS values of all oxabicyclo[3.2.1]octene derivatives in Table S2 show that they are very soluble and soluble in water except **15** compound. Thus, all the oxabicyclo[3.2.1]octene derivatives have good solubility in water and could facilitate well oral adsorption.

All the (**1**–**20**) oxabicyclo[3.2.1]octene derivatives have high gastrointestinal (GI) absorption except **3** compound and non-substrate to P-glycoprotein. Figure 4 illustrates the relationship between TPSA and LogP used in the "Boiled-Egg" model to estimate brain penetration and gastrointestinal absorption of the chosen compounds. The graphic shows that the chemicals **2**, **5**, **7**, **8**, **10**, **13**, **14**, **16**, and **18** are expected to pass through the blood–brain barrier (BBB) in the yellow zone (yolk), while the other oxabicyclo[3.2.1]octene derivatives show a negative response for BBB (in the white).

A molecule will hardly pass through the skin if skin permeability (Log Kp), an important component to take into account for enhancing medicinal efficacy, is greater than 2.5 cm/h. According to Table S2, the Log Kp for oxabicyclo[3.2.1]octene derivatives ranges from 4.55 to 8.04 cm/h (2.5). Therefore, it is reasonable to anticipate that all octene derivatives will effectively permeate skin. Additionally, for all derivatives of oxabicyclo[3.2.1]octenes, synthetic accessibility (SA) values less than 10 indicate that the compounds similar to drugs are relatively simple to synthesize.

Conclusion

The [5+2] cycloaddition reaction between oxidopyrylium **3-OXP** and ethoxyethylene **EthE** yields as products the bridged cyclic ethers and associated seven-membered ring. Theoretical investigation into **P-1x**, **P-1n**, **P-2x**, and **P-2n** has been conducted within the MEDT framework at the computational level DFT/ωB97XD/6-311G(d,p). This 52CA reaction can proceed along 4 isomeric reaction paths and exhibits good regio- and stereoselectivity which improved greatly with the addition of the solvent. An examination of the transition state geometries for the exo and endo stereoisomers indicates that the process of formation of single bonds C1–C4 and C2–C6 and asynchronous, also the asynchronicity increases when the solvent effect of dichloromethane was taken into account. Analysis of the GEDT at the transition points to demonstrate this reaction's weak polarity. According to an ELF topological study of specific locations on the IRC profile of the most advantageous transition state **TS-1x**'s electron density distribution, the reaction will proceed in a non-concerted, two-phase, one-step manner. The coupling of the pseudoradical centers C1 with C4 and C2 with C6 resulted in the development of the novel carbon–carbon, C1-C4 and C2-C6 single bonds.

Supplementary Information The online version contains supplementary material available at https://doi.org/10.1007/s11224-023-02239-4.

Acknowledgements The authors extend their appreciation to the Researchers Supporting Project (number RSP2023R15), King Saud University, Riyadh, Saudi Arabia and we would like to thank Ling Shing Wong for supporting this research.

Author contribution Anas Ouled Aitouna, Abdellah Zeroual: article writing. Abdellah Zeroual and Noureddine Mazoir: numerical calculations; Abdallah M. Elgorban, Ali H. Bahkali, and Asad Syed: acquisition of data; Meenakshi Verma, Radomir Jasiński, and Mohammed El idrissi: final review and editing. All authors: analysis and interpretation of data and drafting the article.

Funding The authors extend their appreciation to the Researchers Supporting Project (number RSP2023R15), King Saud University, Riyadh, Saudi Arabia.

Data availability The authors confirm that the data supporting the findings of this study are available within the article and its supplementary material.

Declarations

Ethics approval The manuscript is prepared in compliance with the Ethics in Publishing Policy as described in the Guide for Authors.

Consent to participate The manuscript is approved by all authors for publication.

Consent for publication The consent for publication was obtained from participants.

Competing interests The authors declare no competing interests.

References

1. Schiavone D V, Kapkayeva DM, Murelli RP (2021) Investigations into a stoichiometrically equivalent intermolecular oxidopyrylium [5+2] cycloaddition reaction leveraging 3-hydroxy-4-pyrone-based oxidopyrylium dimers. J Org Chem 86(5). https://doi.org/10.1021/acs.joc.0c02655
2. Jasiński R (2021) On the question of stepwise [4+2] cycloaddition reactions and their stereochemical aspects. Symmetry (Basel) 13(10). https://doi.org/10.3390/sym13101911
3. Aitouna AO, Barhoumi A, Zeroual A (2023) A mechanism study and an investigation of the reason for the stereoselectivity in the [4+2] cycloaddition reaction between cyclopentadiene and gem-substituted ethylene electrophiles. Sci Radices 2(3):217–228. https://doi.org/10.58332/scirad2023v2i3a01
4. El Ghozlani M, Barhoumi A, Elkacmi R, Ouled Aitouna A, Zeroual A, El idrissi M (2020) Mechanistic study of hetero-Diels-Alder [4+2] cycloaddition reactions between 2-nitro-1H-pyrrole and isoprene. Chemistry Africa 3:901–909. https://doi.org/10.1007/s42250-020-00187-8
5. Zahnoune R, Asserne F, Ourhriss N, Ouled Aitouna A, Barhoumi A, Hakmaoui Y, Belghiti ME, Abouricha S, El ajlaoui R, Zeroual A (2022) Theoretical survey of Diels-Alder between acrylic acid and isoprene catalyzed by the titanium tetrachloride and titanium tertafluoride. J Mol Struct 1269:133630. https://doi.org/10.1016/j.molstruc.2022.133630
6. Aitouna AO, Belghiti ME, Eşme A, Anouar E, Aitouna AO, Zeroual A, Salah M, Chekroun A, El Abdallaoui HE, Benharref A, Mazoir N (2021) Chemical reactivities and molecular docking studies of parthenolide with the main protease of HEP-G2 and SARS-CoV-2. J Mol Struct 130705. https://doi.org/10.1016/j.molstruc.2021.130705
7. Ouled Aitouna Ab, Barhoumi A, El idrissi M, Ouled Aitouna A, Zeroual A, Mazoir N, Chakroun A, Benharref A (2021) Theoretical investigation of the mechanism, chemo- and stereospecifity in the epoxidation reaction of limonene with meta-chloroperoxybenzoic acid (m-CPBA). Mor J Chem 9(1):75–82. https://doi.org/10.48317/IMIST.PRSM/morjchem-v9i1.20462
8. Zeroual A, Ríos-Gutiérrez M, Amiri O, El idrissi M, Domingo LR (2019) An MEDT study of the mechanism, chemo- and stereoselectivity of the epoxidation reaction of R-carvone with peracetic acid. RSC Advances - Royal Society of Chemistry 9:28500–28509. https://doi.org/10.1039/c9ra05309c
9. Raji H, Aitouna AO, Barhoumi A, Chekroun A, Zeroual A, Syed A, Elgorban AM, Verma M, Benharref A, Varma RS (2023) Antiviral docking analysis, semisynthesis and mechanistic studies on the origin of stereo- and chemoselectivity in epoxidation reaction of α′-trans-himachalene. J Mol Liquid 385:122204. https://doi.org/10.1016/j.molliq.2023.122204
10. Breugst M, Reissig HU (2020) The Huisgen reaction: milestones of the 1,3-dipolar cycloaddition. Angew Chemie Int Ed 59(30). https://doi.org/10.1002/anie.202003115
11. Ouahdi Z, Ourhriss N, El idrissi M et al (2022) Exploration of the mechanism, chemospecificity, regiospecificity and stereoselectivity of the cycloaddition reaction between 9α-hydroxyparthenolide and nitrilimine: MEDT study. Theor Chem Acc 141:50. https://doi.org/10.1007/s00214-022-02913-6
12. El idrissi M, El ghozlani M, Eşme A, Ríos-Gutiérrez M, Ouled Aitouna A, Salah M, El Alaoui El Abdallaoui H, Zeroual A, Mazoir N, Domingo LR (2021) Mpro-SARS-CoV-2 inhibitors and various chemical reactivity of 1-bromo- and 1-chloro-4-vinylbenzene in [3+2] cycloaddition reactions. Organics 2:1–16. https://doi.org/10.3390/org2010001
13. Zeroual A, Ríos-Gutiérrez M, El Ghozlani M, El idrissi M, Ouled Aitouna A, Salah M, El Alaoui El Abdallaoui H, Domingo LR (2020) A molecular electron density theory investigation of the molecular mechanism, regioselectivity, stereoselectivity and chemoselectivity of cycloaddition reaction between acetonitrile N-oxide and 2,5-dimethyl-2H-[1,2,3]diazarsole. Theoret Chem Acc 139:37. https://doi.org/10.1007/s12039-019-1656-z
14. Siadati SA (2016) A theoretical study on stepwise- and concertedness of the mechanism of 1, 3-dipolar cycloaddition reaction between tetra amino ethylene and trifluoro methyl azide. Comb Chem High Throughput Screening 19(2):170–175
15. Siadati SA (2016) Beyond the alternatives that switch the mechanism of the 1, 3-dipolar cycloadditions from concerted to stepwise or vice versa: a literature review. Prog React Kinet Mech 41(4):331–344. https://doi.org/10.3184/146867816X14719552202168
16. Zeroual A, Ríos-Gutiérrez M, Salah M, Abdallaoui EAE, H, Domingo LR (2019) An investigation of the molecular mechanism, chemioselectivity and regioselectivity of cycloaddition reaction between acetonitrile N-oxide and 2,5-dimethyl-2H-[1,2,3] diazaphosphole: a MEDT study. J Chem Sci 131:75
17. Al-Rasheed HH, Al-Majid AM, Ali M et al (2022) [3+2] cycloadditions in asymmetric synthesis of spirooxindole hybrids linked to triazole and ferrocene units: X-ray crystal structure and MEDT study of the reaction mechanism. Symmetry (Basel) 14(10). https://doi.org/10.3390/sym14102071
18. Żmigrodzka M, Sadowski M, Kras J, Desler E, Demchuk OM, Kula K (2022) Polar [3+2] cycloaddition between N-methyl azomethine ylide and trans-3,3,3-trichloro-1-nitroprop-1-ene. Sci Radices 01(01). https://doi.org/10.58332/v22i1a02
19. El idrissi M, Eşme A, Hakmaoui Y, Ríos-Gutiérrez M, Ouled Aitouna A, Salah M (2021) A. Zeroual, L. R. Domingo, Divulging the various chemical reactivity of trifluoromethyl-4-vinyl-benzene as well as methyl-4-vinyl-benzene in [3+2] cycloaddition reactions. J Mol Graph Model 102:107760. https://doi.org/10.1016/j.jmgm.2020.107760
20. Mohammad-Salim Haydar A, Ahmed Basheer H, Abdallah HH, Zeroual A, Abdi Jamila L (2021) A molecular electron density theory study for [3+2] cycloaddition reactions of N-benzylcyclohexylnitrone with methyl-3-butenoate. New J Chem 45:262–267. https://doi.org/10.1039/D0NJ04049E
21. Domingo LR, Ríos-Gutiérrez M (2023) A useful classification of organic reactions based on the flux of the electron density. Sci Radices 2:1–24. https://doi.org/10.58332/scirad2023v2i1a01
22. Zawadzińska K, Gostyński B (2023) Nitrosubstituted analogs of isoxazolines and isoxazolidines: a surprising estimation of their biological activity via molecular docking. Sci Radices 2:25–46. https://doi.org/10.58332/scirad2023v2i1a02
23. Salah M, Zeroual A, Jorio S, El Hadki H, Kabbaj O, Marakchi K, Komiha N (2020) Theoretical study of the 1,3-DC reaction between fluorinated alkynes and azides: reactivity indices, transition structures, IGM and ELF analysis. J Mol Graph Model 94:107458. https://doi.org/10.1016/j.jmgm.2019.107458
24. Salah M, Belghiti ME, Aitouna AO, Zeroual A, Jorio S, El Alaoui AH, El Hadki H, Marakchi K, Komiha N (2021) MEDT study of the 1,3-DC reaction of diazomethane with psilostachyin and investigation about the interactions of some pyrazoline derivatives with protease (Mpro) of nCoV-2. J Mol Graph

Model 102:107763. https://doi.org/10.1016/j.jmgm.2020.107763
25. Zeroual A, Ríos-Gutiérrez M, El idrissi M, El Alaoui El Abdallaoui H, Domingo Luis R (2019) An MEDT study of the mechanism and selectivities of the [3+2] cycloaddition reaction of tomentosin with benzonitrile oxide. Int J Quantum Chem 1–9. https://doi.org/10.1002/qua.25980
26. Xiao WL, Yang LM, Gong NB et al (2006) Rubriflordilactones A and B, two novel bisnortriterpenoids from Schisandra rubriflora and their biological activities. Org Lett 8(5). https://doi.org/10.1021/ol060062f
27. Kim E La, Li JL, Hong J et al (2016) An unusual 1(10 → 19)abeo steroid from a jellyfish-derived fungus. Tetrahedron Lett 57(25). https://doi.org/10.1016/j.tetlet.2016.05.050
28. Aoki S, Watanabe Y, Sanagawa M, Setiawan A, Kotoku N, Kobayashi M (2006) Cortistatins A, B, C, D anti-angiogenic steroidal alkaloids, from the marine sponge Corticium simplex. J Am Chem Soc 128(10). https://doi.org/10.1021/ja057404h
29. Nguyen TV, Hartmann JM, Enders D (2013) Recent synthetic strategies to access seven-membered carbocycles in natural product synthesis. Synthesis 45(7). https://doi.org/10.1055/s-0032-1318152
30. Battiste MA, Pelphrey PM, Wright DL (2006) The cycloaddition strategy for the synthesis of natural products containing carbocyclic seven-membered rings. Chem A Eur J 12(13). https://doi.org/10.1002/chem.200501083
31. Pellissier H (2018) Recent developments in the [5+2] cycloaddition. Adv Synth Catal 360(8). https://doi.org/10.1002/adsc.201701379
32. Gao K, Zhang YG, Wang Z, Ding H (2019) Recent development on the [5+2] cycloadditions and their application in natural product synthesis. Chem Commun 55(13). https://doi.org/10.1039/c8cc09077g
33. Yin Z, He Y, Chiu P (2018) Application of (4+3) cycloaddition strategies in the synthesis of natural products. Chem Soc Rev 47(23). https://doi.org/10.1039/c8cs00532j
34. Kącka-Zych A, Jasiński R (2022) Mechanistic aspects of the synthesis of seven-membered internal nitronates via stepwise [4+3] cycloaddition involving conjugated nitroalkenes: molecular electron density theory computational study. J Comput Chem 43(18). https://doi.org/10.1002/jcc.26885
35. Ylijoki KEO, Stryker JM (2013) Cycloaddition reactions in organic and natural product synthesis. Chem Rev 113(3). https://doi.org/10.1021/cr300087g
36. Toda Y, Shimizu M, Iwai T, Suga H (2018) Triethylamine enables catalytic generation of oxidopyrylium ylides for [5+2] cycloadditions with alkenes: an efficient entry to 8-oxabicyclo[3.2.1]octane frameworks. Adv Synth Catal 360(12). https://doi.org/10.1002/adsc.201800290
37. Sammes PG, Street LJ (1983) The preparation and some reactions of 3-oxidopyrylium. J Chem Soc Perkin Trans. https://doi.org/10.1039/p19830001261
38. Zhao C, Glazier DA, Yang D et al (2019) Intermolecular regio- and stereoselective hetero-[5+2] cycloaddition of oxidopyrylium ylides and cyclic imines. Angew Chemie Int Ed 58(3). https://doi.org/10.1002/anie.201811896
39. Bejcek LP, Garimallaprabhakaran AK, Suyabatmaz DM et al (2019) Maltol- and allomaltol-derived oxidopyrylium ylides: methyl substitution pattern kinetically influences [5 + 3] dimerization versus [5+2] cycloaddition reactions. J Org Chem 84(22). https://doi.org/10.1021/acs.joc.9b02137
40. Domingo LR, Zaragozá RJ (2000) Toward an understanding of the mechanisms of the intramolecular [5+2] cycloaddition reaction of γ-pyrones bearing tethered alkenes. A theoretical study. J Org Chem 65(18). https://doi.org/10.1021/jo000061f
41. Zahnoune R, Asserne F, Ourhriss N et al (2022) Theoretical survey of Diels-Alder between acrylic acid and isoprene catalyzed by the titanium tetrachloride and titanium tertafluoride. J Mol Struct 2022:1269. https://doi.org/10.1016/j.molstruc.2022.133630
42. Siadati SA, Rezazadeh S (2022) The extraordinary gravity of three atom 4π-components and 1,3-dienes to C20-nXn fullerenes; a new gate to the future of Nano technology. Sci Radices 01(01). https://doi.org/10.58332/v22i1a04
43. Asserne F, Ouahdi Z, Hakmaoui Y et al (2023) Molecular docking, regio, chemo and stereoselectivity study of the [3+2] cycloaddition reaction between pyridazi-3-one and nitrilimine. Chemistry Africa. https://doi.org/10.1007/s42250-023-00735-y
44. Barhoumi A, Ryachi K, Belghiti ME, Chafi M, Tounsi A, Syed A, El idrissi M, Wong LS, Zeroual A (2023) Chromatography scrutiny, molecular docking, clarifying the selectivities and the mechanism of [3+2] cycloloaddition reaction between linallol and chlorobenzene-nitrile-oxide. J Fluoresc. https://doi.org/10.1007/s10895-023-03411-z
45. Ouled Aitouna AB, Belghiti ME, Eşme A, Ouled Aitouna AN, Salah M, Chekroun A, El Alaoui El Abdallaoui H, Benharref A, Mazoir N, Zeroual A, Nejjari C (2021) Divulging the regioselectivity of epoxides in the ring-opening reaction, and potential himachalene derivatives predicted to target the antibacterial activities and SARS-CoV-2 spike protein with docking study. J Mol Struct 1244:130864. https://doi.org/10.5267/j.ccl.2023.3.008
46. Domingo LR (2016) Molecular electron density theory: a modern view of reactivity in organic chemistry. Molecules 21(10). https://doi.org/10.3390/molecules21101319
47. Seeman JI, Fukui K (2022) Frontier molecular orbital theory, and the Woodward-Hoffmann rules. Part II. A sleeping beauty in chemistry. Chem Rec 22(4). https://doi.org/10.1002/tcr.202100300
48. Becke AD (1990) Edgecombe KE. A simple measure of electron localization in atomic and molecular systems. J Chem Phys 92(9). https://doi.org/10.1063/1.458517
49. Matta CF (2017) On the connections between the quantum theory of atoms in molecules (QTAIM) and density functional theory (DFT): a letter from Richard F. W. Bader to Lou Massa. Struct Chem 28(5). https://doi.org/10.1007/s11224-017-0946-7
50. Johnson ER, Keinan S, Mori-Sánchez P, Contreras-García J, Cohen AJ, Yang W (2010) Revealing noncovalent interactions. J Am Chem Soc 132(18). https://doi.org/10.1021/ja100936w
51. Chai J Da, Head-Gordon M (2008) Long-range corrected hybrid density functionals with damped atom-atom dispersion corrections. Phys Chem Chem Phys 10(44). https://doi.org/10.1039/b810189b
52. Hehre WJ (1976) Ab initio molecular orbital theory. Acc Chem Res 9(11). https://doi.org/10.1021/ar50107a003
53. Fukui K (1981) The path of chemical reactions - the IRC approach. Acc Chem Res 14(12). https://doi.org/10.1021/ar00072a001
54. Tomasi J, Persico M (1994) Molecular interactions in solution: an overview of methods based on continuous distributions of the solvent. Chem Rev 94(7). https://doi.org/10.1021/cr00031a013
55. Parr RG, Szentpály LV, Liu S (1999) Electrophilicity index. J Am Chem Soc 121(9). https://doi.org/10.1021/ja983494x
56. Parr RG, Pearson RG (1983) Absolute hardness: companion parameter to absolute electronegativity. J Am Chem Soc 105(26). https://doi.org/10.1021/ja00364a005
57. Chermette H (1999) Chemical reactivity indexes in density functional theory. J Comput Chem 20:129–154. https://doi.org/10.1002/(SICI)1096-987X(19990115)20:1%3c129::AID-JCC13%3e3.0.CO;2-A
58. Parr G, Yang W (1989) Density-functional theory of atoms and molecules. R Oxford University Press, New York, Oxford
59. Jaramillo P, Domingo LR, Chamorro E, Pérez P (2008) A further exploration of a nucleophilicity index based on the gas-phase ionization potentials. J Mol Struct Theochem 865(1–3). https://doi.org/10.1016/j.theochem.2008.06.022

60. Domingo LR, Aurell MJ, Pérez P, Contreras R (2002) Quantitative characterization of the global electrophilicity power of common diene/dienophile pairs in Diels-Alder reactions. Tetrahedron 58(22). https://doi.org/10.1016/S0040-4020(02)00410-6
61. Reed AE, Weinstock RB, Weinhold F (1985) Natural population analysis. J Chem Phys 83(2). https://doi.org/10.1063/1.449486
62. Noury S, Krokidis X, Fuster F, Silvi B (1999) Computational tools for the electron localization function topological analysis. Comput Chem 23(6):597–604. https://doi.org/10.1016/S0097-8485(99)00039-X
63. Dennington R, Keith TA, Millam JM (2016) GaussView, version 6.0. 16. GaussView, Version 6 Semichem Inc Shawnee Mission KS
64. Humphrey W, Dalke A, Schulten K (1996) VMD: visual molecular dynamics. J Mol Graph 14(1). https://doi.org/10.1016/0263-7855(96)00018-5
65. Borkotoky S (2012) Docking studies on HIV integrase inhibitors based on potential ligand binding sites. Int J Bioinforma Biosci 2(3):21–29. https://doi.org/10.5121/ijbb.2012.2303
66. Morris GM, Ruth H, Lindstrom W et al (2009) AutoDock4 and AutoDockTools4: automated docking with selective receptor flexibility. J Comput Chem 30(16):2785–2791. https://doi.org/10.1002/JCC.21256
67. Morris GM, Goodsell DS, Halliday RS et al (1998) Automated docking using a Lamarckian genetic algorithm and an empirical binding free energy function. J Comput Chem 19(14). https://doi.org/10.1002/(SICI)1096-987X(19981115)19:14<1639::AID-JCC10>3.0.CO;2-B
68. Delano WL (2002) The PyMOL molecular graphics system. CCP4 Newsl Protein Crystallogr 40(1)
69. Daina A, Michielin O, Zoete V (2017) SwissADME: a free web tool to evaluate pharmacokinetics, drug-likeness and medicinal chemistry friendliness of small molecules. Sci Rep 7. https://doi.org/10.1038/srep42717
70. Lipinski CA (2004) Lead- and drug-like compounds: the rule-of-five revolution. Drug Discov Today Technol 1(4):337–341. https://doi.org/10.1016/J.DDTEC.2004.11.007
71. Guan L, Yang H, Cai Y et al (2019) ADMET-score – a comprehensive scoring function for evaluation of chemical drug-likeness. Medchemcomm 10(1):148–157. https://doi.org/10.1039/C8MD00472B